International Journal of Biological Macromolecules 222 (2022) 1996–2005

Contents lists available at ScienceDirect

International Journal of Biological Macromolecules

journal homepage: www.elsevier.com/locate/ijbiomac

Effect of hydrolysis time, pH and surfactant type on stability of hydrochloric acid hydrolyzed nanocellulose

D. Pawcenis [a,*], M. Leśniak [b], M. Szumera [b], M. Sitarz [b], J. Profic-Paczkowska [a]

[a] Faculty of Chemistry, Jagiellonian University, Gronostajowa 2, 30-387 Kraków, Poland
[b] AGH University of Science and Technology, Faculty of Materials Science and Ceramics, 30-059 Kraków, Poland

ARTICLE INFO

Keywords:
Nanocellulose
Cellulose nanocrystals
Cellulose nanofibers
Hydrochloric acid hydrolysis
Surfactants

ABSTRACT

Nanocelluloses are the subject of much interest on the account of their mechanical properties, high surface area, porosity, etc. Typically, sulfuric acid is used to produce cellulose nanocrystals with high aspect ratio and dispersibility in water suspensions. However, hydrolysis in sulfuric acid leads to cellulose esterification, which has some drawbacks such as lower thermal stability of nanocellulose. Hydrochloric acid does not cause functionalization of the nanocellulose surface, yet yields in poor colloidal stability in aqueous solutions due to the lack of ionic interactions between CNC/CNF and water molecules. Therefore, it should be possible to tune the colloidal stability of nanocellulose aqueous suspensions by modifying the properties of the solution (such as pH and/or the presence of surfactants). In this work, we attempted to obtain stable aqueous CNF suspensions via hydrochloric acid hydrolysis. Hydrolysis was performed at three time intervals, at 60 °C temperature and 6 mol/dm^3 of hydrochloric acid. To find the optimum stabilizing conditions, the effect of different pH values and various surfactants on CNF stability was explored. The best stabilizing effect was observed at pH range 5–9 and in nonionic surfactant. The obtained products were characterized by using spectroscopic (FTIR), microscopic (AFM), thermogravimetric and X-ray diffraction techniques.

1. Introduction

Cellulose is a major component of naturally occurring composite - wood, containing approx. 50 % of cellulose, 30 % of lignin and 20 % of hemicelluloses. As renewable biopolymers are being studied because of the need to reduce consumption of non-renewable petroleum products, cellulose is emerging as an important raw material. Furthermore, cellulose composites have been developed into nanocomposites, in which nanocellulose acts as a reinforcement, stimuli-responsive filler or dispersing agent in, for example, mechanically adaptive polymer nanocomposites, novel carbon materials and other applications [1–5]. In fact, nanocellulose is a term that refers to cellulose nanofibers, bacterial nanocellulose and cellulose nanocrystals (CNCs) [6,7]. The nano dimensions result in a high surface area, porosity and hence the interactions of nanocelluloses with other molecules, such as water, other polymeric compounds and nanoparticles [8]. Cellulose nanofibers are formed from wood pulp by mechanical processing assisted with chemical or enzymatic treatment, and are characterized by a diameter of 5–60 nm and several micrometers length. Cellulose nanocrystals are typically produced via acid hydrolysis of cellulose originated from different sources (plants, bacteria or algae). They are characterized by similar dimensions to CNFs, but their length varies from roughly 100 to 250 nm. Although their size is similar to CNF, CNCs have limited flexibility, as they do not contain amorphous domains but instead exhibit crystalline rod-like shapes. Among mineral acids, predominantly sulfuric acid at concentration 64 % is used for different source cellulose (tunicate, wood or bacterial) hydrolysis because it provides the resulting cellulose nanocrystals with nanometric dimensions and good stability in aqueous suspensions [9–12]. Colloidal stability of CNCs obtained by sulfuric acid hydrolysis is explained by the presence of negatively charged sulfate groups introduced by esterification of surface hydroxyl groups. Both stability and aggregation state can be modified by ionic strength, pH or the presence of particular metal cations with different valency [13]. On the other hand, introducing sulfate groups can lead to a decrease of thermal stability of CNCs [14,15]. Another mineral acid, phosphoric acid, has been used to produce thermally stable CNCs [16–18]. Kusmono and Affan evaluated the yield and properties of nanocellulose extracted from Ramie fibers by using phosphoric acid solutions [18]. The obtained nanocellulose was characterized with crystalline structure typical for cellulose I, and this observation

* Corresponding author.
E-mail address: d.pawcenis@uj.edu.pl (D. Pawcenis).

https://doi.org/10.1016/j.ijbiomac.2022.09.289
Received 6 July 2022; Received in revised form 9 September 2022; Accepted 30 September 2022
Available online 5 October 2022

indicated that phosphoric acid hydrolysis did not affect crystal structure of substrate cellulose. Nevertheless, the optimized experimental conditions required performing the hydrolysis at 150 °C, which is relatively harsh in comparison to "traditional|" hydrolysis with sulfuric acid (between 45 and 60 °C) [19]. Work by Espinosa et al. compared properties of CNCs obtained via hydrolysis of three different mineral acids: sulfuric acid (S-CNC), hydrochloric acid (H-CNC) and phosphoric (P-CNC) [16]. It was demonstrated that, even at low charge density (arising from the small number of surface -PO_4^{3-} groups), cellulose nanocrystals P-CNC were stable in various polar solvents such as DMSO, DMF and water. Thermal stability was also evaluated, and it was increasing in the following order: S-CNC < P-CNC < H-CNC. The authors explained the better thermal stability of P-CNC compared to S-CNC by lower degree of esterification and thus lower charge density. Apparently, the degree of esterification is difficult to control in the case of sulfuric acid hydrolysis. Nevertheless, it is worth noting that, among the aforementioned three mineral acids, hydrolysis with HCl provides cellulosic products with the highest thermal stability. The onset of decomposition temperature for both H-CNC and P-CNC was 220 °C, but the maximum decomposition temperature was 15–25 °C lower for P-CNC. This study highlights the relationship between the charge density and thermal stability of cellulose nanocrystals. Hydrolysis performed with hydrochloric acid does not cause esterification of cellulose hydroxyl groups, although such CNCs tend to aggregate and are characterized with poor stability because of pronounced hydrogen bonding between their hydroxyl groups. Consequently, they are difficult to disperse in solvents. This issue can be overcome by the addition of inorganic ions, surfactants, or the application of ultrasounds [11,13,20–22]. Ultrasound irradiation is used both at the pre-treatment stage of cellulose fiber extraction as well as a hydrolysis supporting treatment [23].

An interesting work on the application of acidified $ZnCl_2$ molten salt for the hydrolysis of cellulose was presented recently by Shen et al. [24]. By applying specific concentrations of $ZnCl_2$ and HCl as well as cellulose to liquid ratio, CNCs with tunable morphology and allomorphs were obtained. Another non-conventional approach to mineral acid-assisted hydrolysis of cellulose is the use of HCl vapors for cellulose hydrolysis and thus nanocellulose extraction [25,26]. In this study, cellulose fibers were exposed to hydrochloric vapors and underwent degradation and crystallization without change of the cellulose sample texture. However, extensive sonication (72 h) in formic acid was required to achieve dispersion to nanocrystalline suspension. As the authors claimed, this work was a proof of concept for tuning the supramolecular properties of heterogeneous materials in solid state.

The addition of surfactants to nanocellulose can be an appealing alternative to chemical modification of the nanocellulose's surface. Stabilization with the use of surfactants can be achieved by purely physical adsorption of a surfactant on the nanocellulose by surface entropic effects, hydrogen bonding, hydrophilic-hydrophobic and charge–charge interactions [27]. Some recent works present attempts at stabilization of hydrochloric acid hydrolyzed cellulose nanocrystals (H-CNCs) with the use of common surfactants [21,28,29]. Shang et al. reported a study on developing H-CNC (hydrochloric acid hydrolyzed cellulose nanocrystal) stabilized with cationic surfactant CTAB followed by ultrasound treatment. [21] It was demonstrated that stable hydrochloric acid-hydrolyzed CNCs can be obtained by adsorbing CTAB at low concentration (below critical micellization concentration) on CNC surface [21,30]. Surfactant at a concentration below its CMC is adsorbed at the CNC surface, thus providing the steric hindrance, whereas the above surfactant's CMC micelles are formed, which in turn do not enable suppression of cellulose nanocrystal aggregation. Similarly, cationic modification with CTAB was also successfully applied to sulfuric acid-hydrolyzed cellulose nanocrystals extracted from sago fronds [31]. Kaboorani and Riedl demonstrated the tunability of CNC hydrophobicity by proper selection of the modifying surfactant (in this case, hexadecyltrimethylammonium bromide) concentration [29]. Noteworthy was that the modification improved the dispersibility of CNC in low polarity solvents such as THF. Importantly, no loss in the reinforcing capability of the products was noted, since such modification did not alter the crystallite structure and dimensions. Concerning nonionic surfactants, particular attention should be paid to amphiphilic block polymers-derived surfactants. Pluronics are particularly interesting in terms of different modes of their adsorption on the nanocellulose's surface. Adsorption behavior can be tuned by length of hydrophilic and hydrophobic segments. Typically, poly(ethylene oxide) blocks indicate high affinity to hydrophilic surface of nanocellulose, whereas segments interact with aqueous surrounding [32].

Other factors greatly affecting the stability of various CNC aqueous dispersions (for example, S-CNC, TEMPO-oxidized nanocellulose and cellulose nanofibrils) are the solution's pH and temperature. This is especially important for applications such as drilling fluids' enhanced oil recovery (EOR) [33–35]. In the case of anionic ester groups on the nanocellulose's surface, their ionization is dependent on pH value. Thus, the aggregation and stability of colloidal CNC dispersion can be predicted based on DLVO theory, which assumes that, between colloidal particles, various forces occur. These are Van der Waals and electrical double layer forces. This electrical double layer may consist of: i) a layer of electrons ii) a layer of adsorbed ions/ionic groups on the solid surface iii) a diffused double layer consisting of ions, where ions of one sign prevail over the other. In the case of anionic ester groups such as those occurring on the surface of sulfuric acid-hydrolyzed CNC particles, excess of one type of ions may govern the aggregation behavior of nanocrystalline cellulose dispersion [35]. Furthermore, Way et al. showed the various impact of pH on mechanical properties of CNC-based nanocomposites dependent on the type of CNC surface modification: with carboxylic acid (-COOH) and amine groups (-NH_2) [4]. For instance, the opposite effect of low pH on tensile storage moduli was observed for CNC-COOH (increase) and CNC-NH_2 (decrease) based nanocomposites. This example clearly highlights the significance of pH value on the numerous parameters of CNCs in solution and solid state.

Judging by the number of literature reports so far, most attention of research on nanocrystalline cellulose is focused on CNCs obtained by hydrolyzing cellulose in concentrated sulfuric acid, whereas the number of works dedicated to improving stability of CNCs from hydrochloric acid hydrolysis seems to be still modest. Unlike for other CNC-based materials, not much is known about the influence of pH and ionic strength on the stability of aqueous solutions of HCl-hydrolyzed CNCs. Although stabilization of such CNCs with cationic surfactants has been described in the literature, there is still a gap in the knowledge about the influence of anionic and non-ionic surfactants on the stabilization of hydrochloric acid-hydrolyzed CNCs. Furthermore, to our best knowledge, the effect of pH on the properties of HCl-hydrolyzed CNCs in solution was not elaborated either.

The main objective of this work was to obtain stable HCl-hydrolyzed cellulose nanofibers in aqueous solution. To achieve this, hydrochloric acid hydrolysis and consecutively short sonochemical treatment were applied. The effect of different time of hydrolysis, pH values and type of surfactant (cationic (hexadecyltrimethylammonium bromide, CTAB), anionic (sodium dodecyl sulfate, SDS) and nonionic (Pluronic F- 127, PF-127)) on the colloidal and thermal stability, chemical and crystalline structure as well as morphology was assessed. The range of experimental parameters allowed their impact on the resulting materials properties to be assessed.

2. Materials and methods

2.1. Materials and reagents

Unsized handmade cover paper made from hemp and linen textiles (Conservation by Design, UK) was used as the cellulose source. Hydrochloric acid (35–38 %) and sodium hydroxide (pellets, pure for analysis) were purchased from POCh (Gliwice, Poland). Surfactants (CTAB, SDS, PF-127) were purchased from Acros Organics, Roth and Sigma

respectively. All chemicals were used as received without additional purification.

2.2. Hydrochloric acid hydrolysis of cellulose

Cellulose sheets were carefully hand torn, stratified and cut in small pieces approx. 5 × 5 mm. 40 mL of 6 M HCl was added to each beaker, and the beakers were then placed in a water bath on a magnetic plate at 60 °C. When the temperature of HCl reached the set temperature, 1 g of cellulose was added to each beaker containing 40 mL of 6 M HCl. Hydrolysis was carried out at 60 °C for 90, 180 and 270 min under magnetic stirring. After the specified time elapsed, hydrolysis was quenched by diluting the cellulose suspension with 1 L of cold deionized water. The suspension was centrifuged for 40 min at 3000 x*g*. The resulting supernatant was washed with deionized water and centrifuged again. The procedure was repeated until reaching neutral pH, indicating removal of hydrochloric acid. The washed product was vacuum-filtered and redispersed in deionized water at concentration 2 % (*w/v*), denoted as stock solution. The stock solutions were prepared for each time of hydrolysis (90, 180, 270). Then, CNFs at 1 % concentration were prepared from the particular stock solutions.

2.3. Preparation of sonicated cellulose nanofiber colloidal solutions

CNF suspensions at different pH values were prepared by adjusting pH to 3, 5, 7, 9 and 11 using hydrochloric acid and sodium hydroxide 0.5 M solutions. An appropriate volume of surfactants (CTAB, SDS, PF-127) was added to 2 mL of 1 % CNF so that their final concentration was equal to half of critical micellization concentration at 25 °C (see Table 1). Samples are described accordingly in Table 1, and their IDs are a combination of hydrolysis time and pH value or surfactant type. For instance, the sample denoted as 180.11 means cellulose hydrolyzed for 180 min and adjusted to pH 11.

Suspensions containing 1 % (w/v) of CNF at given pH or upon addition of particular surfactant were then subjected to ultrasound treatment. All samples were sonicated at a frequency of 20 kHz, with an amplitude of 100 %, and the average power 90 W for 60 s (Qsonica S-4000). Only 60 s of sonication was sufficient to obtain viscous, opaque suspensions. The scheme of whole procedure is presented in Fig. 1.

2.4. Characterization of CNFs in solid and solution state

Part of each CNF solution was freeze-dried (−85 °C, 0.5 mbar, Lyo-Quest −85, Telstar) to obtain solid product necessary for spectroscopic, X-ray diffraction and thermal stability characterization. Infrared spectra were recorded using a THERMO/Nicolet 8700 spectrometer with MCT/A detector equipped with ATR appliance (Golden Gate, Specac). Prior to FTIR measurement, all samples were kept in an air oven at 105 °C to remove residual water. For the purpose of crystallinity index comparison between various samples, all spectra were normalized using the internal standard method (integral of the CH_2 band between 2800 and 3000 cm^{-1}) described in our previous works [36–39]. The crystallinity index was calculated from absorbance ratio between 1426 cm^{-1} and 895 cm^{-1} bands [40].

X-ray diffraction experiments were carried out with use of an X'PertPro MPD diffractometer (Phillips), equipped with a Johansson monochromator with copper $K\alpha_1$ line ($\lambda = 1.5405$ Å) and a silicon, position sensitive X'Celerator detector. Measurements were performed in Bragg-Brentano θ–2θ geometry in the range of 2θ 5–60°, increment of 0.016°/min and time of 175.26 s for each angular step. During measurements, a variable divergence slit was used to allow constant sensitivity to be obtained through the whole range of 2θ. Crystallinity indexes were calculated with the Gaussian peaks fitting method, assuming the presence of five Gaussian peaks for the crystalline phase and one Gaussian peak for the amorphous phase [41]. Once the peak areas were calculated from the peak fitting, CI was determined accordingly to Eq. (1):

$$CI = 1 - \frac{A_{amorphous}}{A_{total}} \quad (1)$$

where $A_{amorphous}$ is the area of the amorphous cellulose peak, and A_{total} is the total area of all peaks (five crystalline and one amorphous).

The thermal behavior of samples was studied with an STA 449 F3 Jupiter (NETZSCH) operating in DSC mode. Three milligram samples were analyzed in open Pt crucibles. The DSC and TGA measurements were carried out at a temperature range of 30–600 °C, and at a heating rate of 10 °C/min under flowing nitrogen atmosphere (40 mL/min). Al_2O_3 was used as the reference material. Thermal curves were evaluated with Netzsch Proteus software.

Liquid samples were subjected to viscometric (room temperature, SV-10 vibro-viscometer, A&D Company) and zeta potential measurements (DLS Malvern Zetasizer Nano ZS, Malvern, UK, equipped with an He—Ne laser). Measurements were done in triplicate.

Investigations of CNF morphology and size measurements were performed using an atomic force microscope (AFM, XE-100 system, Park Systems, South Korea; separated x–y and z scanner, scan size: 5 × 5 μm). with ultra-sharp silicon tip (<10 nm) mounted on a cantilever with Al reflective coating. For AFM experiments, a small droplet of CNF suspension was diluted with DI water, applied on clean mica surface (highest quality grade V1 mica, 0.21 mm {0.0085″} thickness; TedPella, USA) and left to dry overnight. The AFM measurements were performed in tapping mode. Statistical analysis and preparation of images of topographies were carried out using the XEI software (Park System, South Korea) and Fiji software. Average diameters and lengths were calculated from at least 100 measurements using Fiji software. The significance of differences between the measured values was evaluated by using one-way analysis of the variance (ANOVA) and the Tukey test ($\alpha = 0.05$).

Redispersibility of freeze-dried CNF samples was evaluated by dissolving CNF samples in deionized water. CNF samples were mixed with water and then vortexed to obtain 1 % (*w/v*) CNF solution. The photographs were taken right after preparing solution and after 24 h.

Table 1
Sample nomenclature according to hydrolysis time and set value of pH or type of surfactant used.

pH/surfactant	Time of hydrolysis, minutes		
	90	180	270
3	90.3	180.3	270.3
5	90.5	180.5	270.5
7	90.7	180.7	270.7
9	90.9	180.9	270.9
11	90.11	180.11	270.11
CTAB (0.45 mmol/L)	90.CTAB	180.CTAB	270.CTAB
SDS (C = 4 mmol/L)	90.SDS	180.SDS	270.SDS
PF-127 (C = 2.9 mmol/L)	90.PF-127	180.PF-127	270.PF-127

3. Results and discussion

3.1. Properties of CNFs in solution

As already presented in Fig. 1, nanocellulose obtained directly via HCl hydrolysis quickly undergoes sedimentation and two separate phases are clearly visible, independently of pH, surfactant presence and hydrolysis time. Subjecting those solutions to sonication yields visually homogeneous, viscous suspensions that are stable for an undetermined time. In this particular study, the obtained solutions retained their viscosity and opacity for at least six months. Indeed, viscosity may be considered as a measure of polymer colloidal stability, as well as enabling changes in the colloidal state of polymer solutions to be monitored. Fig. 2 presents changes in the dynamic viscosities of CNF solutions after 90, 180 and 270 min of hydrolysis (Fig. 2 A-C, top orange

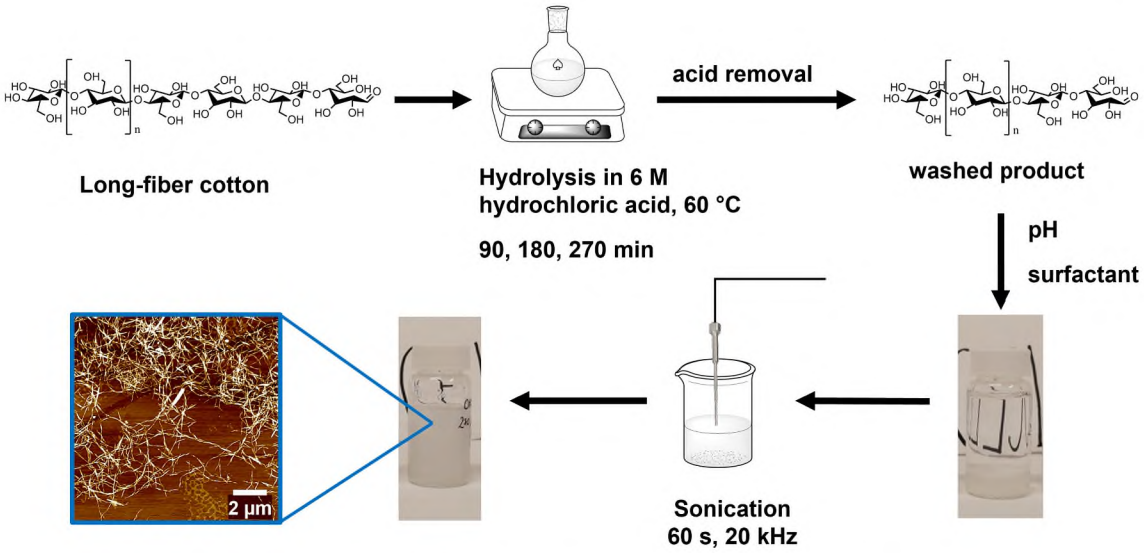

Fig. 1. Procedure of nanocellulose extraction using hydrochloric acid hydrolysis followed by ultrasound treatment.

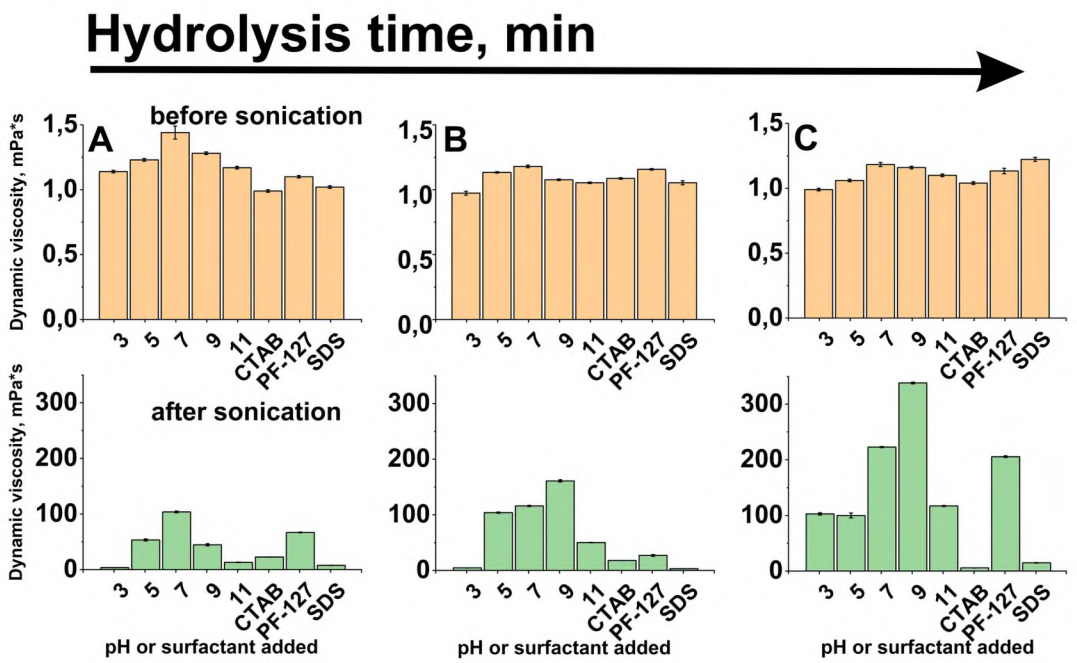

Fig. 2. Dynamic viscosities changes before (orange) and after (green) sonication of CNF solutions obtained via hydrolysis for A. 90 min, B. 180 min, C. 270 min. (For interpretation of the references to colour in this figure legend, the reader is referred to the web version of this article.)

column graphs) and after application of ultrasound (the green column graphs below the corresponding orange ones). With increasing time of hydrolysis, no significant changes are observed when considering series without sonication (Fig. 2 A-C before sonication). Average viscosities are typical for dilute aqueous solutions of cellulose. Upon sonication, even a 100 to 300-fold increase in viscosity occurs (Fig. 2 A-C, bottom green column graphs). Additionally, an impact of particular pH on solution viscosity was noticed. A pronounced increase is noted for samples at pH 9 hydrolyzed at longer time intervals (180.9 and 270.9), whereas for solutions at pH 3, the increase is observed only after 270 min of hydrolysis. Regarding the shortest hydrolysis time, the highest increase in viscosity is noticed at pH 7 and in solution containing nonionic surfactant – PF-127. This might indicate that, under these conditions, short-range forces (such as hydrogen bonds or van der Waals forces) govern the interaction between CNF molecules and the surfactant under these conditions.

Concerning longer time intervals of hydrolysis, significantly higher viscosity of solutions at pH 9 may result from increasing size of nanocellulose particles resulting from their aggregation. Additionally, in an alkaline environment, cellulose starts to dissolve and gain effective charge, which may lead to viscosity increase [42].

Surface charge of CNFs, determined by means of ζ potential (electrokinetic potential), indicates some variations depending on hydrolysis time, pH and surfactant nature. It is worth noting that data for CNF solution only after sonication are presented (Fig. 3), because high fluctuation of signal was observed for samples before sonication, due to CNF particle sedimentation. In general, all sonicated formulations are characterized with negative values of ζ potential, regardless on pH or surfactant type. The highest negative values were observed in the case of CNF hydrolyzed for 180 min and stabilized with PF-127. This value (c. a.

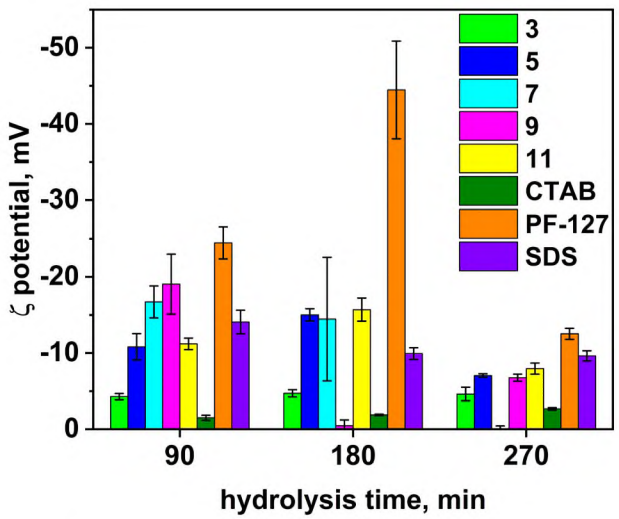

Fig. 3. Zeta potential changes with increased hydrolysis time.

−44 mV) is typical for stable systems, where no aggregation occurs [43]. Neutral CNF suspensions such as those at pH 7 (7.90 and 7.180) are characterized with ζ potential between −20 and −10 mV, which indicates that the surface of CNF crystals is negatively charged also under neutral pH. Furthermore, positive charge of CTAB is suppressed by this negative charge of CNF and consequently CNF dispersions such as CTAB. 90, 180 and 270, which are characterized with only slightly charged surfaces undergo aggregation.

As concerns the effect of solution pH on electrokinetic potential of CNF, it is clearly seen that, in acidic conditions (pH 3: 90.3, 180.3 and 270.3), mean ζ potential value remains constant regardless of hydrolysis time, and is equal to c.a. −4.3 to −4.7 mV. With decreased concentration of H_3O^+ and thus higher pH, an increase in ζ potential can be observed with maximum at pH 7 and 9 for samples treated with 90 min of hydrolysis. With longer hydrolysis time, this trend decays. Surprisingly, a dramatic drop of ζ potential for CNF at pH 9 (180.9 and 270.9) occurs, which could be attributed to CNF aggregation as discussed for dynamic viscosity results. A similar trend is observed for sample series at pH 7, where an increase in dynamic viscosity occurs in parallel with ζ potential decrease. Furthermore, ζ potential for CNF at pH 5 changes only mildly with increased hydrolysis time, and this trend is in accordance with dynamic viscosity changes. Therefore, it can be concluded that longer time of hydrolysis leads to CNF aggregation at neutral and alkaline pH. Concerning the surfactant stabilized CNFs, the optimum time of hydrolysis is between 90 and 180 min, especially for nonionic surfactant PF-127.

3.2. Morphology characteristics of CNFs using AFM

Because nanocelluloses are typically characterized with the high aspect ratio, particle size distribution cannot be measured by dynamic light scattering (DLS) [44]. Consequently, it is rather recommended to perform particle size analysis by microscopic techniques such as AFM.

The applied treatments (hydrolysis time and sonication) and solution parameters (pH and surfactant type) were expected to affect the morphology of resulting CNF samples significantly. It can be seen that the smallest diameters were noted for most of the samples after hydrolysis for 180 min (Fig. 4 A and B). For instance, sample 5.180 was characterized with average diameter 56 nm. It must be highlighted here that the difference in measured diameter values for 5.90 and 5.180 (66 and 56 nm respectively) is not statistically significant. In the group of surfactant-stabilized CNFs, the smallest diameters were observed for samples PF-127.90 and PF-127.180, which were equal to 88 and 84 nm respectively, and the difference in the mean values is not statistically significant, likewise for 5.90 and 5.180. After 270 min of hydrolysis, average diameter values increased to 73 nm (5.270) and 104 nm (PF-127.270), and this increase is statistically significant. However, it means that, after longer times of hydrolysis (yielding smaller CNFs particles),

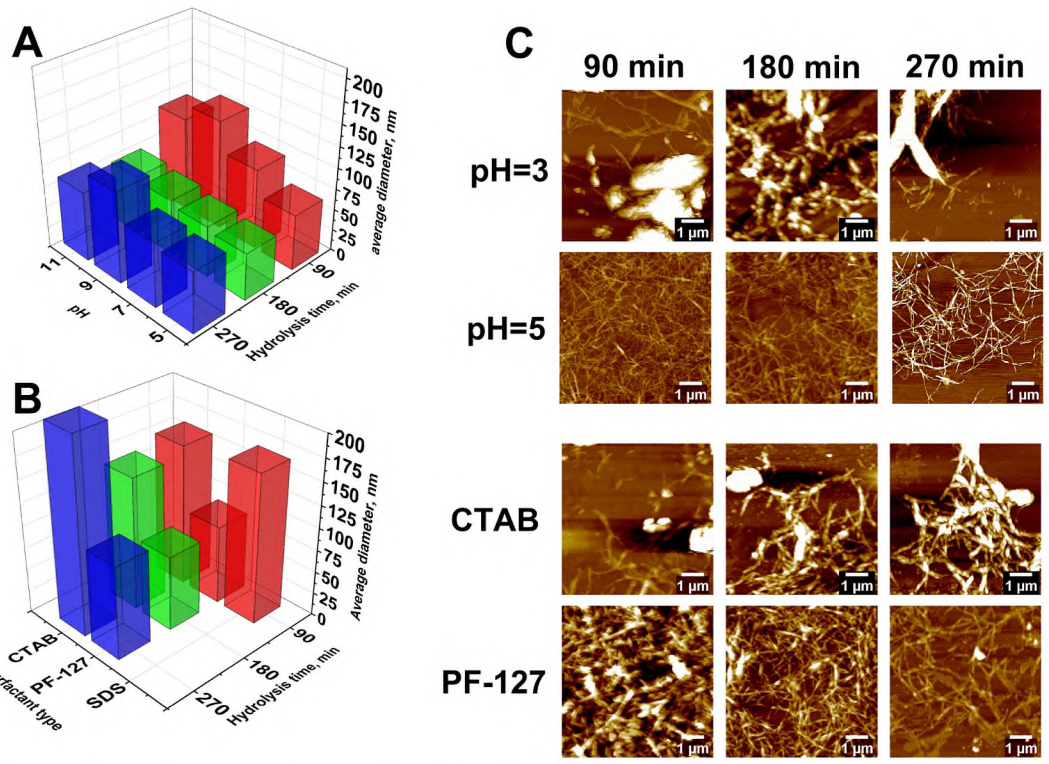

Fig. 4. Average diameters as function of hydrolysis time and A. pH of CNF solution B. type of surfactant added, C. Selected AFM height images of extracted nanocellulose fibers (scale bars – 1 μm).

aggregation may occur, leading to an apparent increase in mean diameter. Moreover, for CNF samples hydrolyzed for a shorter time (90 min), large standard deviations of determined diameters were noticed (e.g. 66 ± 56 nm for 5.90 sample). This indicates broader distribution of CNF diameters, which can be ascribed to the coexistence of hydrolyzed and unhydrolyzed cellulose fragments [45]. It is noteworthy that electrokinetic potential measurements showed that the optimum hydrolysis time was 90 and 180 for pH-modified and PF-127-stabilized samples. In the case of the AFM technique, observations are in agreement with colloidal stability results from ζ-potential analyses: cellulose nanofibers with the smallest diameters (and therefore indicating the lowest aggregation) were observed for samples that were subjected to 180 min of hydrolysis.

What draws particular attention is the fact that, at the lowest pH, nanocellulose tends to aggregate and form clumps upon water evaporation (Fig. 4 C), and only a few separated fibers could be observed. Similar observations were made for samples stabilized with 180.SDS, 270.SDS and 270.CTAB. The AFM images of all samples are presented in Fig. S2.

Aspect ratios (expressed as length to diameter ratio) in general increased as the hydrolysis time increased to 180 min, after which they decreased (Table 2). Similar observations were reported by other authors [46–48]. The maximum value of L/D ratio was determined for sample 5.180, and it was equal to 21. Although the average diameter of 180.5 and 90.5 CNFs are similar, their average lengths values are significantly different, so that sample 90.5 is characterized with much lower aspect ratio equal to 8.38. For all CNF samples, a broad distribution of average length was observed and did not become narrower with longer hydrolysis time (unlike average diameter). Interestingly, for PF-127-stabilized CNFs, aspect ratios increased linearly with increasing hydrolysis time of cellulose. The average diameter of nanocellulose fibers increased with longer hydrolysis times (due to some extent of aggregation as mentioned before), and the average lengths of the fibers also increased. Because PF-127 was added to the CNF suspension after hydrolysis, this length increase could be related again to aggregation or specific interaction between CNFs and PEO (poly(ethylene oxide)) or the PPO (poly(propylene oxide)) segment of PF-127. Noteworthy is that the PF-127 concentration used in this study is below its critical micellization concentration in order to avoid micellization of PF-127, which would potentially in turn prevent CNF – PF-127 interactions. Interactions between nanocellulose and PF-127 is not electrostatic but rather short-range hydrophilic and hydrophobic ones [49]. According to previous studies, PEO forms hydrogen bonding owing to the presence of ether oxygen in the monomer and hydroxyl groups on cellulose, so PPO may create loops between PEO blocks adsorbed on the CNC surface [49,50]. Therefore, apparent elongation of CNFs stabilized with PF-127 may result from some kind of "wrapping" of several CNFs by PF-127 molecules. This may also be the origin of the colloidal stability of PF-127-stabilized CNFs, as revealed by ζ potential study in the Section 3.1. *Properties of CNFs in solution*. Nevertheless, the spatial arrangement of CNFs and PF-127 molecules in solution is not fully understood, and requires further studies.

Table 2
Average diameters, lengths and aspect ratios of selected cellulose nanofibers with standard deviations in brackets.

Sample ID	D, nm (±)	L, nm (±)	L/D
90.5	66 (56)	803 (234)	8.38
180.5	56 (20)	1185 (492)	21
270.5	73 (16)	1000 (441)	13.7
PF-127.90	88 (22)	540 (252)	6.14
PF-127.180	84 (29)	787 (251)	9.4
PF-127.270	104 (27)	1394 (480)	13.4

3.3. Structural and thermal properties of CNFs

3.3.1. Crystallinity changes and hydrogen network reorganization evidenced by XRD and FTIR

Diffraction patterns of all cellulose samples indicate cellulose in the form of Iβ polymorph, even in the case of samples sonicated in alkaline aqueous environment (See fig. S1). On this basis, it can be assumed that the crystalline structure of cellulose remained intact independently of hydrolysis time, sonication and the composition of suspensions. In general, in the group of pH-modified CNF samples, the average crystallinity index oscillates between 0.87 and 0.94. This means a CI increase of >20 % compared to cellulose substrate (CI = 0.64). Beside the fact that acidic hydrolysis leads to the removal of the amorphous phase in cellulose, particular concentration of H_3O^+ and OH^- ions contributes to the reorganization of the hydrogen bond network. At high pH, ionization of the nanocellulose -OH group may also play a role to some extent [51]. Interesting observations were made in the case of surfactant-stabilized CNF samples. Samples stabilized with ionic surfactant are characterized with high values of CI (0.83 to 0.93) similarly to pH-modified samples, whereas PF-127-stabilized samples reveal noticeably lower crystallinity, with maximum value equal to 0.86 for 270.PF-127. This can be ascribed to a different mode of nonionic surfactant interaction with nanocellulose surface as compared to the interactions between ionic surfactants and nanocelluloses. As discussed before, CNF molecules may be interspersed with hydrophobic PPO segments of the PF-127 chain, leading to distortion of nanocellulose crystalline structure. Similar observations were reported for nanocellulose modified with other nonionic surfactants [52,53]. In turn, ionic surfactants used in this study were characterized with much lower molecular weight, and thus contact area with CNF surfaces was possibly much lower than in the case of PF-127.

Changes in cellulose structure were evaluated by means of the ATR FTIR technique. Since this technique gives an insight into surface and subsurface structure, all spectra were normalized prior to semi-quantitative interpretation (Fig. S3). The normalization procedure assumes a constant number of methylene -CH_2 groups in all cellulosic samples, which is assigned as C6 of the glucopyranose ring (absorption band between 3000 and 2800 cm^{-1}). For this reason, spectra of CNF samples with added surfactants were not subjected to the normalization procedure, as -CH_2 groups from, for example, SDS alkyl chains of surfactants interrupt quantitative interpretation. Therefore, FTIR spectra recorded for CNFs stabilized with surfactants (Fig. S3 G-I) were not analyzed regarding crystallinity changes.

Concerning the potential impact of hydrolysis on cellulose structure, no evolution of new bands was observed (Fig. S3 A – F). None of the cellulose-specific bands were found to disappear either. However, the spectra differ in the intensity of the individual bands (Fig. S3). The broad absorption bands between 3600 and 3000 cm^{-1} are ascribed to the –OH bond stretching, and the bands at 1640 cm^{-1} are typical for O—H bending vibrations of adsorbed water in cellulosic materials. A band at 1160 cm^{-1}, corresponding to glycosidic stretching vibration (C—O), changed its relative intensity and is the lowest after 270 min of hydrolysis, which is associated with the most pronounced depolymerization of cellulose chain and is in accordance with the expected result. Overall, the chemical structure of cellulose was not altered by hydrolysis, which is in agreement with previous reports [54–56].

Crystalline indexes from FTIR can be elucidated on the basis of the absorbance ratio between the 1426 cm^{-1} and 895 cm^{-1} bands, which correspond to —CH_2 symmetrical bending and C—O valence vibrations, respectively. The band at 1426 cm^{-1} is sensitive to changes in the environment of C6 atoms, such as the formation or disruption of hydrogen bonds. The band at 895 cm^{-1} is assigned to the vibrations of atoms bound to C1 atom, therefore it can be a marker of molecular conformation changes resulting from the rotation within C1—O—C4 bonding (glycosidic bond) [40]. Thus, the relative absorbance intensity of those two bands can be treated as a measure of crystalline structure

order in cellulose molecules. These indexes cannot be regarded as an absolute measure of crystallinity, but are sometimes used to track changes in a particular set of samples [57,58]. As demonstrated in one of our previous works, CI calculated on the basis of ATR FTIR and XRD techniques were in a good correlation ($r = 0.97$) in the case of amorphous cellulose samples [39].

Calculated CI_{FTIR} are summarized in Fig. 5C and Table S1 in Supplementary Information. It is clearly seen that the crystallinity index determined with use of FTIR significantly increased upon acid hydrolysis followed by sonication when comparing these values to the CI of cellulose used as a substrate (CI = 0.99, see Fig. 5C and Table S1). Since the band at 895 cm^{-1} reflects the glycosidic bond environment, it is obvious that its intensity decreases during acid hydrolysis. On one hand, breaking of glycosidic bond contributes to the increase in the 1426 to 895 cm^{-1} band ratio. On the other hand, the presence of various concentrations of H_3O^+ and OH^- ions (expressed as pH) contributes to reorganization of hydrogen bonds, which may proceed in a very complicated way. This in turn leads to changes of 1426 cm^{-1} band intensity and the observation of different trends of CI changes. For the set of acidified CNF samples (90.3, 180.3 and 270.3 series), growth of CI value to 1.53 can be noticed. However, longer time of hydrolysis does not cause further increase in CI and the maximum value is reached after 180 min of hydrolysis (Fig. 5A-C). In the case of CNFs with pH 5 maximum CI is also reached after 180 min and longer hydrolysis leads to drop of the crystallinity. This might result from disruption or formation of new hydrogen bonds at C6, and consequently a decrease of their vibration intensity was observed. Another trend is noticed for the 90.7, 180.7 and 270.7 set, where a steady decrease of CI occurs, starting from 1.77 for 90.7 and ending at 1.08 for 270.7. It can be hypothesized that, in this series, the main change occurs within C6 group, as the intensity of the corresponding band decreases significantly. Opposite to each other, trends are observed for CNF at the pH 9 and 11 series, where maximum CI values are reached after 270 and 90 min, respectively. In the case of the CNF at pH 9 series (90.9, 180.9 and 270.9), this trend may result from more pronounced depolymerization in the alkaline environment, additionally enhanced by sonication. In the case of the 90.11, 180.11 and 270.11 CNF series, a drop of the $A_{1426/895}$ ratio might be caused again by the reorganization of the hydrogen-bonding network around the C6 group and —OH groups ionization, but rather not by cellulose mercerization, as for mercerization the minimum required concentration of NaOH is 0.25 mol/L [51].

3.3.2. *Thermal stability and behavior of PF-127 stabilized nanocellulose fibers*

Based on ζ potential, viscosity and crystallinity studies, only PF-127-stabilized CNF samples were subjected to thermal property studies (Fig. 6 A and B).

The sharp DTG peaks centered at 50 °C, corresponding to a weight loss of 2.3 %, were due to the evaporation of adsorbed water (Fig. 6 A) from cellulose and surfactant stabilized-CNFs samples.

The DTG peaks between 358 and 361 °C for cellulose and surfactant-stabilized CNFs are present due to cellulose degradation processes. Surfactant PF-127 alone indicates a higher onset degradation temperature as well as higher temperature at the maximum weight loss rate (T_{max}) when comparing to cellulose-based samples (see Fig. 6 A, green data series). Regarding residual mass at 600 °C, the least mass loss (and thus the highest thermal stability) among hydrolyzed samples is observed for the 90.PF-127 sample. With increasing hydrolysis time (samples 180.PF-127 and 270.PF-127), an increase in weight loss is noticed. T_{max} values, derived from DTG peak maxima (Fig. 6 A, dashed data set, Table S2), also shift slightly towards lower temperatures with longer hydrolysis time. Substrate cellulose is characterized by somewhat higher onset degradation temperature and T_{max} compared to CNFs, which is a quite obvious and expected observation. Moreover, its mass loss at 600 °C is higher than that observed for hydrolyzed sample 90.PF-127. Thermal decomposition of acid hydrolysis products is affected by several parameters including hydrolysis conditions, cellulose degree of polymerization and crystallinity index [59]. It can be assumed that average degree of polymerization (DP) decreases with increasing hydrolysis time. So, according to work by Agustin et al. [60] and Gurgel et al. [59], samples with lower DP indicate lower T_{max}. Some authors tried to explain the decrease in thermal stability by the decrease in the crystallinity index occurring together with decreasing DP [61]. However, Agustin et al. observed the opposite relation between hydrolysis time (and consequently DP) and crystallinity index, and they attribute the decrease in thermal stability with decreasing DP to the increase in the number of reducing ends of cellulose molecules [60]. The highest residual mass at the end of the heating (and thus, indirectly, higher thermal stability) for the 90.PF-127 sample can be explained by the lesser extent of depolymerization among the set of PF-127-stabilized samples.

It is noteworthy that samples 90 to 270 stabilized with PF-127 indicate a pronounced hump of the TG curve in the temperature range of 100–300 °C. It must be highlighted that all experiments were performed in a nitrogen atmosphere, therefore no oxidation could occur. Differential scanning calorimetry (DSC) curves in Fig. 6 B do not indicate any peak in this range, therefore an oxidation reaction of CNFs is excluded. This broad hump is not observed for substrate cellulose and PF-127, which suggests that apparent mass increase in the discussed temperature range might be related somehow to the nanocrystalline properties of CNFs. Explaining this observation requires more analyses of a wide range of different types of nanocellulose samples, and should be subject to a separate study.

3.4. *Redispersibility of freeze-dried CNF*

Drying of cellulose materials is known to cause irreversible reorganization of hydrogen bondings in cellulose thus leading to the difficulties with dispersion of dried cellulosic material. This reorganization originates from the fact that the removal of H_2O during drying, shortens the distance between two individual nanocellulose particles [62,63]. The shortened distance leads to the increase in Van der Waals force between

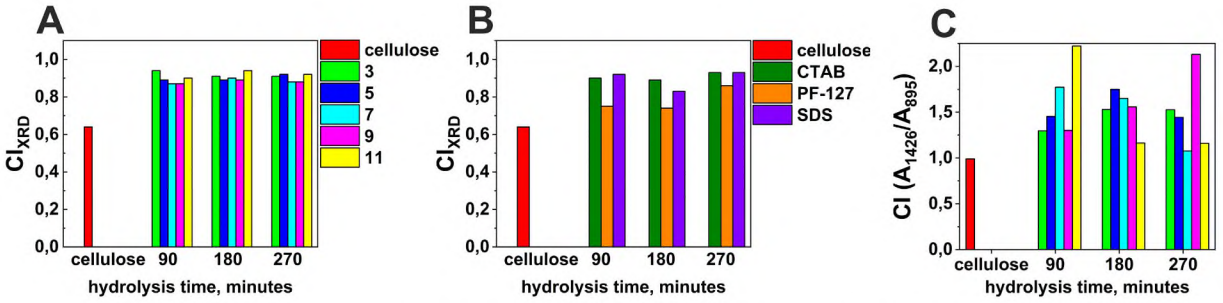

Fig. 5. Crystallinity index (from XRD) changes in function of hydrolysis time and: A. pH of solution; B. type of surfactant; C. crystallinity index (from FTIR) in function of hydrolysis time and pH. A common legend is used for picture A and C.

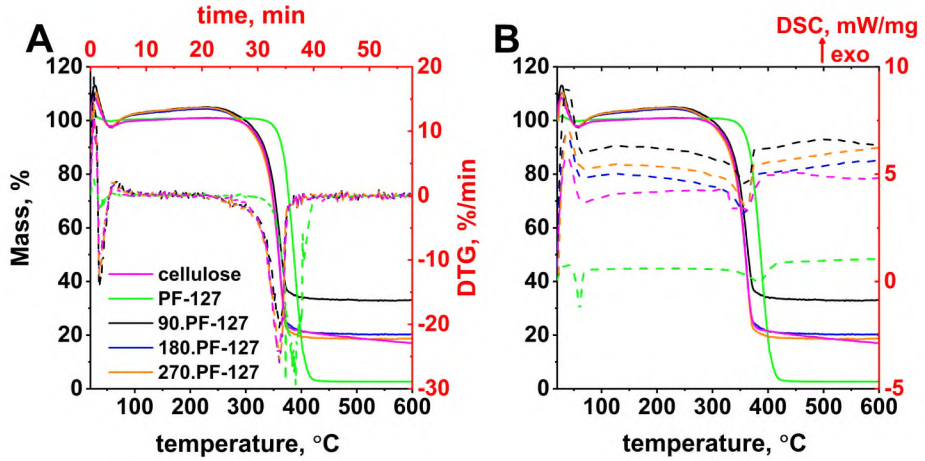

Fig. 6. A. TG and DTG curves of substrate cellulose, PF-127 and stabilized CNFs, B. TG and DSC overlay of cellulose, PF-127 and stabilized CNFs. Note that graphs A and B have a common legend.

cellulose fibrils, and results in the formation of interfibrillar hydrogen bonds that cannot be disrupted upon nanocellulose re-wetting [64]. The strategies for improving nanocellulose dispersibility (thus prevent nanocellulose from aggregation) upon dehydration include surface charge modification, steric hindrance by bulky groups and other approaches like solvent exchange. In the case of this study, surfactant (SDS, CTSB and PF-127) stabilized CNF samples are an example of steric hindrance approach. CNF suspensions in medium with various pH cannot be considered as classical "surface charge" modified, however some charge modification occurs as revealed by ξ – potential experiments. Stability of redispersed freeze-dried CNF samples are depicted in the Fig. 7 A. In general, CNF solutions at higher pH (9 and above) indicated higher rate of sedimentation. This may be ascribed to repulsion between slightly negatively charged surface of CNF and OH^- ions in the alkaline solution. Oppositely, the number of hydrogen bonds, that were formed during freeze-drying of CNF, in acidic pH can be effectively reduced owing to ion–dipole interactions. Among studied samples, the lowest sedimentation rate was observed for CNF sample 270.5, for which individualized nanofibers could be observed by AFM technique (See Fig. 7 B). Moderate rate of sedimentation was noticed for CNF hydrolyzed for 90 and 180 min and with pH fixed at 7. In neutral pH longer time of hydrolysis resulted in aggregation of CNF upon redispersing in water. Additionally to long time of hydrolysis, lower concentration of H_3O^+ may lead to less efficient screening of hydroxyl groups of CNF. This could lead to more pronounced formation of interfibrillar hydrogen bonds.

Regarding surfactants stabilized CNF, stabilization of CNF was not achieved even in the case of PF-127. This observation may suggest that surfactants' concentration (half of critical micellization concentration), that initially was sufficient to stabilize CNF, may be not adequate to provide the stability of redispersed CNF. Therefore, further optimization of CNF and surfactants (in particular PF-127) composition is essential to prove (or deny) that surfactants can be used to obtain redispersible CNF.

4. Conclusions

In this work, we presented systematic study of nanocellulose extraction from long fiber cotton using hydrochloric acid followed by sonication, and we described the effect of various solution parameters on the physicochemical properties of the product nanocellulose. Individualized nanocellulose whiskers were obtained by applying hydrochloric acid, short-time sonication and particular solution parameters, without esterification of hydroxyl groups in cellulose. For the first time, the effect of a wide range of pH and surfactant type on colloidal stability of CNF solutions was demonstrated. Different hydrolysis time followed by adjusting concentration of H_3O^+ ions, type of surfactant and sonication make it possible to obtain individualized cellulose nano-whiskers with high aspect ratio and crystallinity index. Additionally, it was proved that CNF samples, which were hydrolyzed for up to 10 min and with pH fixed between 5 and 7 were characterized with the best colloidal stability. Among surfactants, best colloidal stability was noticed for samples hydrolyzed for up to 180 min and then stabilized with PF-127. Importantly, neither hydrolysis conditions nor pH/surfactant modification change the functional groups of cellulose molecule, as confirmed by ATR-FTIR technique. A high degree of crystallinity was confirmed both by ATR-FTIR and XRD techniques, while morphology of nano-

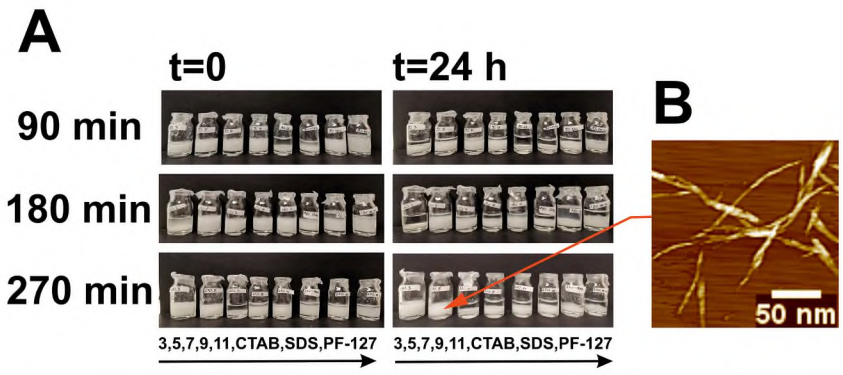

Fig. 7. A. Stability of redispersed CNF samples hydrolyzed for 90, 180 and 270 min. Left column presents suspensions right after preparing the solutions ($t = 0$), column on the right side shows the same samples after 24 h ($t = 24$ h). B. AFM image of 270.5 CNF sample.

whiskers was elucidated from AFM. For pH-modified CNF suspensions, the highest aspect ratio was found for CNFs hydrolyzed for 180 min and with pH fixed at 5. Among surfactant stabilized CNFs, nano-whiskers hydrolyzed for 270 min were characterized with the highest aspect ratio. The results are important for the rational design of nanocellulose-based composites and tailoring their properties. Preliminary results for CNF redispersibility in selected conditions indicate possibility to stabilize nanocellulose in aqueous solutions using easily available and cheap agents. In turn, the interactions between surfactants (in particular PF-127) and nanocellulose require further studies to fully understand the binding mode of a surfactant on nanocellulose surface and to improve redispersibility of such stabilized CNF.

CRediT authorship contribution statement

Dominika Pawcenis: Conceptualization, Methodology, Formal analysis, Investigation, Writing – original and revised draft, Funding acquisition. **Magdalena Leśniak**: Investigation, Writing – original draft. **Magdalena Szumera**: Investigation, Writing – original draft. **Maciej Sitarz**: Investigation. **Joanna Profic-Paczkowska**: Writing – original draft.

Declaration of competing interest

The authors declare that they have no known competing financial interests or personal relationships that could have influenced the work reported in this paper.

Acknowledgements

Financial support from the National Science Centre (SONATA 12, decision No. 2016/23/D/ST5/00451) is kindly acknowledged. The research was carried out with the equipment purchased thanks to the financial support of the European Regional Development Fund within the framework of the Polish Innovation Economy Operational Program (contract number POIG.02.01.00-12-023/08).

Appendix A. Supplementary data

Supplementary data to this article can be found online at https://doi.org/10.1016/j.ijbiomac.2022.09.289.

References

[1] I. Caulfield, The structures of cellulose, in: D.F. Caulfield, J.D. Passaretti, S. F. Sobczynski (Eds.), Mater. Interact. Relev. to Pulp, Pap. Wood Ind. Proceedings, Mater. Res. Soc. Symp, Materials Research Society, Pittsburgh, 1990, pp. 89–98.
[2] D. Klemm, D. Schumann, F. Kramer, N. Heßler, M. Hornung, H.P. Schmauder, S. Marsch, Nanocelluloses as innovative polymers in research and application, Adv. Polym. Sci. 205 (2006) 49–96, https://doi.org/10.1007/12_097.
[3] A. Hajian, S.B. Lindström, T. Pettersson, M.M. Hamedi, L. Wågberg, Understanding the dispersive action of nanocellulose for carbon nanomaterials, Nano Lett. 17 (2017) 1439–1447, https://doi.org/10.1021/acs.nanolett.6b04405.
[4] A.E. Way, L. Hsu, K. Shanmuganathan, C. Weder, S.J. Rowan, PH-responsive cellulose nanocrystal gels and nanocomposites, ACS Macro Lett. 1 (2012) 1001–1006, https://doi.org/10.1021/mz3003006.
[5] D.C. Wang, H.Y. Yu, D. Qi, Y. Wu, L. Chen, Z. Li, Confined chemical transitions for direct extraction of conductive cellulose nanofibers with graphitized carbon shell at low temperature and pressure, J. Am. Chem. Soc. 143 (2021) 11620–11630, https://doi.org/10.1021/jacs.1c04710.
[6] D. Klemm, B. Heublein, H.P. Fink, A. Bohn, Cellulose: fascinating biopolymer and sustainable raw material, Angew. Chem.Int. Ed. 44 (2005) 3358–3393, https://doi.org/10.1002/anie.200460587.
[7] D. Klemm, F. Kramer, S. Moritz, T. Lindström, M. Ankerfors, D. Gray, A. Dorris, Nanocelluloses: a new family of nature-based materials, Angew. Chem.Int. Ed. 50 (2011) 5438–5466, https://doi.org/10.1002/anie.201001273.
[8] D. Klemm, D. Schumann, F. Kramer, N. Hebler, D. Koth, B. Sultanova, Nanocellulose materials - different cellulose, different functionality, Macromol. Symp. 280 (2009) 60–71, https://doi.org/10.1002/masy.200950608.
[9] S.A. Ogundare, V. Moodley, W.E. van Zyl, Nanocrystalline cellulose isolated from discarded cigarette filters, Carbohydr. Polym. 175 (2017) 273–281, https://doi.org/10.1016/j.carbpol.2017.08.008.
[10] X. An, Y. Wen, D. Cheng, X. Zhu, Y. Ni, Preparation of cellulose nano-crystals through a sequential process of cellulase pretreatment and acid hydrolysis, Cellulose 23 (2016) 2409–2420, https://doi.org/10.1007/s10570-016-0964-4.
[11] T.I. Shaheen, H.E. Emam, Sono-chemical synthesis of cellulose nanocrystals from wood sawdust using acid hydrolysis, Int. J. Biol. Macromol. 107 (2018) 1599–1606, https://doi.org/10.1016/j.ijbiomac.2017.10.028.
[12] I.A. Sacui, R.C. Nieuwendaal, D.J. Burnett, S.J. Stranick, M. Jorfi, C. Weder, E. J. Foster, R.T. Olsson, J.W. Gilman, Comparison of the properties of cellulose nanocrystals and cellulose nanofibrils isolated from bacteria, tunicate, and wood processed using acid, enzymatic, mechanical, and oxidative methods, ACS Appl. Mater. Interfaces 6 (2014) 6127–6138, https://doi.org/10.1021/am500359f.
[13] L. Zhong, S. Fu, X. Peng, H. Zhan, R. Sun, Colloidal stability of negatively charged cellulose nanocrystalline in aqueous systems, Carbohydr. Polym. 90 (2012) 644–649, https://doi.org/10.1016/j.carbpol.2012.05.091.
[14] N. Wang, E. Ding, R. Cheng, Thermal degradation behaviors of spherical cellulose nanocrystals with sulfate groups, Polymer (Guildf.) 48 (2007) 3486–3493, https://doi.org/10.1016/j.polymer.2007.03.062.
[15] M. Roman, W.T. Winter, Effect of sulfate groups from sulfuric acid hydrolysis on the thermal degradation behavior of bacterial cellulose, Biomacromolecules 5 (2004) 1671–1677, https://doi.org/10.1021/bm034519+.
[16] S. Camarero Espinosa, T. Kuhnt, J. Foster, C. Weder, Isolation of thermally stable cellulose nanocrystals by phosphoric acid hydrolysis, Biomacromolecules 14 (2013) 1223–1230. https://doi.org/10.32604/jrm.2020.07940.
[17] J. Araki, M. Wada, S. Kuga, T. Okano, Flow properties of microcrystalline cellulose suspension prepared by acid treatment of native cellulose, Colloids Surf.A Physicochem. Eng. Asp. 142 (1998) 75–82, https://doi.org/10.1016/S0927-7757(98)00404-X.
[18] Kusmono, M.N. Affan, Isolation and characterization of nanocrystalline cellulose from ramie fibers via phosphoric acid hydrolysis, J. Nat. Fibers 19 (2020) 2744–2755, https://doi.org/10.1080/15440478.2020.1821292.
[19] H. Kargarzadeh, M. Ioelovich, I. Ahmad, S. Thomas, A. Dufresne, Methods for Extraction of Nanocellulose From Various Sources, Wiley-VCH Verlag GmbH & Co. KGaA, 2017, https://doi.org/10.1002/9783527689972.ch1.
[20] N. Pandi, S.H. Sonawane, K. Anand Kishore, Synthesis of cellulose nanocrystals (CNCs) from cotton using ultrasound-assisted acid hydrolysis, Ultrason. Sonochem. 70 (2021), 105353, https://doi.org/10.1016/j.ultsonch.2020.105353.
[21] Z. Shang, X. An, F.T. Seta, M. Ma, M. Shen, L. Dai, H. Liu, Y. Ni, Improving dispersion stability of hydrochloric acid hydrolyzed cellulose nano-crystals, Carbohydr. Polym. 222 (2019), 115037, https://doi.org/10.1016/j.carbpol.2019.115037.
[22] T. Cao, M. Elimelech, Colloidal stability of cellulose nanocrystals in aqueous solutions containing monovalent, divalent, and trivalent inorganic salts, J. Colloid Interface Sci. 584 (2021) 456–463, https://doi.org/10.1016/j.jcis.2020.09.117.
[23] W. Chen, H. Yu, Y. Liu, P. Chen, M. Zhang, Y. Hai, Individualization of cellulose nanofibers from wood using high-intensity ultrasonication combined with chemical pretreatments, Carbohydr. Polym. 83 (2011) 1804–1811, https://doi.org/10.1016/j.carbpol.2010.10.040.
[24] C. Shen, C. Hu, W. Zhang, X. Lin, W. Qi, Acidified - ZnCl2 molten salt hydrate systems as hydrolytic media for cellulose I and II nanocrystal production: from rods to spheres, Cellulose 29 (2022) 7629–7647, https://doi.org/10.1007/s10570-022-04712-5.
[25] E. Kontturi, A. Meriluoto, P.A. Penttilä, N. Baccile, J.M. Malho, A. Potthast, T. Rosenau, J. Ruokolainen, R. Serimaa, J. Laine, H. Sixta, Degradation and crystallization of cellulose in hydrogen chloride vapor for high-yield isolation of cellulose nanocrystals, Angew. Chem.Int. Ed. 55 (2016) 14455–14458, https://doi.org/10.1002/anie.201606626.
[26] M. Lorenz, S. Sattler, M. Reza, A. Bismarck, E. Kontturi, Cellulose nanocrystals by acid vapour: towards more effortless isolation of cellulose nanocrystals, Faraday Discuss. 202 (2017) 315–330, https://doi.org/10.1039/c7fd00053g.
[27] B.L. Tardy, S. Yokota, M. Ago, W. Xiang, T. Kondo, R. Bordes, O.J. Rojas, Nanocellulose–surfactant interactions, Curr. Opin. Colloid Interface Sci. 29 (2017) 57–67, https://doi.org/10.1016/j.cocis.2017.02.004.
[28] N. Dhar, D. Au, R.C. Berry, K.C. Tam, Interactions of nanocrystalline cellulose with an oppositely charged surfactant in aqueous medium, Colloids Surf.A Physicochem. Eng. Asp. 415 (2012) 310–319, https://doi.org/10.1016/j.colsurfa.2012.09.010.
[29] A. Kaboorani, B. Riedl, Surface modification of cellulose nanocrystals (CNC) by a cationic surfactant, Ind. Crop. Prod. 65 (2015) 45–55, https://doi.org/10.1016/j.indcrop.2014.11.027.
[30] N. Dhar, D. Au, R.C. Berry, K.C. Tam, Interactions of nanocrystalline cellulose with an oppositely charged surfactant in aqueous medium, Colloids Surf.A Physicochem. Eng. Asp. 415 (2012) 310–319, https://doi.org/10.1016/j.colsurfa.2012.09.010.
[31] I.W. Arnata, S. Suprihatin, F. Fahma, N. Richana, T.C. Sunarti, Cationic modification of nanocrystalline cellulose from sago fronds, Cellulose 27 (2020) 3121–3141, https://doi.org/10.1007/s10570-019-02955-3.
[32] Y. Li, H. Liu, J. Song, O.J. Rojas, J.P. Hinestroza, Adsorption and association of a symmetric PEO-PPO-PEO triblock copolymer on polypropylene, polyethylene, and cellulose surfaces, ACS Appl. Mater. Interfaces 3 (2011) 2349–2357, https://doi.org/10.1021/am200264r.
[33] E.B. Heggset, G. Chinga-Carrasco, K. Syverud, Temperature stability of nanocellulose dispersions, Carbohydr. Polym. 157 (2017) 114–121, https://doi.org/10.1016/j.carbpol.2016.09.077.
[34] S.N. Molnes, K.G. Paso, S. Strand, K. Syverud, The effects of pH, time and temperature on the stability and viscosity of cellulose nanocrystal (CNC) dispersions: implications for use in enhanced oil recovery, Cellulose 24 (2017) 4479–4491, https://doi.org/10.1007/s10570-017-1437-0.

[35] W. Qi, J. Yu, Z. Zhang, H.-N. Xu, Effect of pH on the aggregation behavior of cellulose nanocrystals in aqueous medium, Mater. Res. Express 6 (2019), 125078.
[36] J. Łojewska, P. Miskowiec, L.M. Proniewicz, Oxidative and hydrolytic path of paper degradation studied by in-situ ftir transmission spectroscopy, in: Durab. Pap. Writ, 2004, pp. 24–25.
[37] J. Łojewska, P. Miśkowiec, T. Łojewski, L.M. Proniewicz, Cellulose oxidative and hydrolytic degradation: in situ FTIR approach, Polym. Degrad. Stab. 88 (2005) 512–520, https://doi.org/10.1016/j.polymdegradstab. 2004.12.012.
[38] J. Łojewska, A. Lubańska, P. Miśkowiec, T. Łojewski, L.M. Proniewicz, FTIR in situ transmission studies on the kinetics of paper degradation via hydrolytic and oxidative reaction paths, Appl. Phys. A Mater. Sci. Process. 83 (2006) 597–603, https://doi.org/10.1007/s00339-006-3529-9.
[39] M. Mattonai, D. Pawcenis, S. del Seppia, J. Łojewska, E. Ribechini, Effect of ball-milling on crystallinity index, degree of polymerization and thermal stability of cellulose, Bioresour. Technol. 270 (2018) 270–277, https://doi.org/10.1016/j.biortech.2018.09.029.
[40] M.L. Nelson, R.T. O'Connor, Relation of certain infrared bands to cellulose crystallinity and crystal lattice type. Part II. A new infrared ratio for estimation of crystallinity in celluloses I and II, J. Appl. Polym. Sci. 8 (1964) 1325–1341, https://doi.org/10.1002/app.1964.070080323.
[41] S. Park, J.O. Baker, M.E. Himmel, P.A. Parilla, D.K. Johnson, Cellulose crystallinity index: measurement techniques and their impact on interpreting cellulase performance, Biotechnol. Biofuels 3 (2010) 10, https://doi.org/10.1186/1754-6834-3-10.
[42] E. Bialik, B. Stenqvist, Y. Fang, Å. Östlund, I. Furó, B. Lindman, M. Lund, D. Bernin, Ionization of cellobiose in aqueous alkali and the mechanism of cellulose dissolution, J. Phys. Chem. Lett. 7 (2016) 5044–5048, https://doi.org/10.1021/acs.jpclett.6b02346.
[43] S. Samimi, N. Maghsoudnia, R.B. Eftekhari, F. Dorkoosh, Lipid-Based Nanoparticles for Drug Delivery Systems, Elsevier Inc., 2018, https://doi.org/10.1016/B978-0-12-814031-4.00003-9.
[44] E.J. Foster, R.J. Moon, U.P. Agarwal, M.J. Bortner, J. Bras, S. Camarero-Espinosa, K.J. Chan, M.J.D. Clift, E.D. Cranston, S.J. Eichhorn, D.M. Fox, W.Y. Hamad, L. Heux, B. Jean, M. Korey, W. Nieh, K.J. Ong, M.S. Reid, S. Renneckar, R. Roberts, J.A. Shatkin, J. Simonsen, K. Stinson-Bagby, N. Wanasekara, J. Youngblood, Current characterization methods for cellulose nanomaterials, Chem. Soc. Rev. 47 (2018) 2609–2679, https://doi.org/10.1039/c6cs00895j.
[45] P. Spiliopoulos, S. Spirk, T. Paakkonen, M. Viljanen, K. Svedstrom, L. Pitkanen, M. Awais, E. Kontturi, Visualizing degradation of cellulose nanofibers by acid hydrolysis, Biomacromolecules 22 (2021) 1399–1405, https://doi.org/10.1021/acs.biomac.0c01625.
[46] H. Kargarzadeh, I. Ahmad, I. Abdullah, A. Dufresne, S.Y. Zainudin, R.M. Sheltami, Effects of hydrolysis conditions on the morphology, crystallinity, and thermal stability of cellulose nanocrystals extracted from kenaf bast fibers, Cellulose 19 (2012) 855–866, https://doi.org/10.1007/s10570-012-9684-6.
[47] Y. Chen, C. Liu, P.R. Chang, X. Cao, D.P. Anderson, Bionanocomposites based on pea starch and cellulose nanowhiskers hydrolyzed from pea hull fibre: effect of hydrolysis time, Carbohydr. Polym. 76 (2009) 607–615, https://doi.org/10.1016/j.carbpol.2008.11.030.
[48] M. Martínez-Sanz, A. Lopez-Rubio, J.M. Lagaron, Optimization of the nanofabrication by acid hydrolysis of bacterial cellulose nanowhiskers, Carbohydr. Polym. 85 (2011) 228–236, https://doi.org/10.1016/j.carbpol.2011.02.021.
[49] E. Kushan, E. Senses, Thermoresponsive and injectable composite hydrogels of cellulose nanocrystals and pluronic F127, ACS Appl. Bio Mater. 4 (2021) 3507–3517, https://doi.org/10.1021/acsabm.1c00046.
[50] D. Cheng, Y. Wen, L. Wang, X. An, X. Zhu, Y. Ni, Adsorption of polyethylene glycol (PEG) onto cellulose nano-crystals to improve its dispersity, Carbohydr. Polym. 123 (2015) 157–163, https://doi.org/10.1016/j.carbpol.2015.01.035.
[51] B.J.C. Duchemin, Mercerisation of cellulose in aqueous NaOH at low concentrations, Green Chem. 17 (2015) 3941–3947, https://doi.org/10.1039/c5gc00563a.
[52] C.J. Wijaya, S. Ismadji, H.W. Aparamarta, S. Gunawan, Hydrophobic modification of cellulose nanocrystals from bamboo shoots using rarasaponins, ACS Omega 5 (2020) 20967–20975, https://doi.org/10.1021/acsomega.0c02425.
[53] J.N. Putro, S. Ismadji, C. Gunarto, F.E. Soetaredjo, Y.H. Ju, Effect of natural and synthetic surfactants on polysaccharide nanoparticles: hydrophobic drug loading, release, and cytotoxic studies, Colloids Surf.A Physicochem. Eng. Asp. 578 (2019), 123618, https://doi.org/10.1016/j.colsurfa.2019.123618.
[54] A.A. Dimas, W.W.Muhammad Kusmono, N.I. Mochammad, Extraction and characterization of nanocrystalline cellulose (Ncc) from ramie fiber by hydrochloric acid hydrolysis, Key Eng. Mater. 867 (2020) 109–116, https://doi.org/10.4028/www.scientific.net/KEM.867.109. KEM.
[55] M.M. Mahmud, A. Perveen, R.A. Jahan, M.A. Matin, S.Y. Wong, X. Li, M.T. Arafat, Preparation of different polymorphs of cellulose from different acid hydrolysis medium, Int. J. Biol. Macromol. 130 (2019) 969–976, https://doi.org/10.1016/j.ijbiomac.2019.03.027.
[56] N. Hastuti, K. Kanomata, T. Kitaoka, Hydrochloric acid hydrolysis of pulps from oil palm empty fruit bunches to produce cellulose nanocrystals, J. Polym. Environ. 26 (2018) 3698–3709, https://doi.org/10.1007/s10924-018-1248-x.
[57] M. Schwanninger, J.C. Rodrigues, H. Pereira, B. Hinterstoisser, Effects of short-time vibratory ball milling on the shape of FT-IR spectra of wood and cellulose, Vib. Spectrosc. 36 (2004) 23–40, https://doi.org/10.1016/j.vibspec.2004.02.003.
[58] M. Szymańska, J. Hoppe, M. Dutkiewicz, P. Sobolewski, M. Palacz, E. Janus, B. Zielińska, R. Drozd, Silicone polyether surfactant enhances bacterial cellulose synthesis and water holding capacity, Int. J. Biol. Macromol. 208 (2022) 642–653, https://doi.org/10.1016/j.ijbiomac.2022.03.124.
[59] L.V.A. Gurgel, K. Marabezi, L.A. Ramos, A.A.da S. Curvelo, Characterization of depolymerized residues from extremely low acid hydrolysis (ELA) of sugarcane bagasse cellulose: effects of degree of polymerization, crystallinity and crystallite size on thermal decomposition, Ind. Crops Prod. 36 (2012) 560–571, https://doi.org/10.1016/j.indcrop.2011.11.009.
[60] M.B. Agustin, F. Nakatsubo, H. Yano, The thermal stability of nanocellulose and its acetates with different degree of polymerization, Cellulose 23 (2016) 451–464, https://doi.org/10.1007/s10570-015-0813-x.
[61] M.E. Calahorra, M. Cortázar, J.I. Eguiazábal, G.M. Guzmán, Thermogravimetric analysis of cellulose: effect of the molecular weight on thermal decomposition, J. Appl. Polym. Sci. 37 (1989) 3305–3314, https://doi.org/10.1002/app.1989.070371203.
[62] H.W. Kwak, J. You, M.E. Lee, H.J. Jin, Prevention of cellulose nanofibril agglomeration during dehydration and enhancement of redispersibility by hydrophilic gelatin, Cellulose 26 (2019) 4357–4369, https://doi.org/10.1007/s10570-019-02387-z.
[63] M. Nordenström, T. Kaldéus, J. Erlandsson, T. Pettersson, E. Malmström, L. Wågberg, Redispersion strategies for dried cellulose nanofibrils, ACS Sustain. Chem. Eng. 9 (2021) 11003–11010, https://doi.org/10.1021/acssuschemeng.1c02122.
[64] Y. Xu, Y. Xu, H. Chen, M. Gao, X. Yue, Y. Ni, Redispersion of dried plant nanocellulose: a review, Carbohydr. Polym. 294 (2022), 119830, https://doi.org/10.1016/j.carbpol.2022.119830.